Electronic Supplementary Material (ESI) for Physical Chemistry Chemical Physics.
This journal is © the Owner Societies 2020

Supplementary Material for

Interfacial tension and mechanism of liquid-liquid phase separation in aqueous media

Amber R. Titus, Luisa A. Ferreira, Alexander I. Belgovsky, Edgar E. Kooijman, Elizabeth K. Mann, J. Adin Mann Jr., William V. Meyer, Anthony E. Smart, Vladimir N. Uversky, Boris Y. Zaslavsky*

* Boris Y. Zaslavsky
Email: Boris.Zaslavsky@cleveland-diagnostics.com

This PDF file includes:

Materials and Methods
Supplementary Text
Figures S1 to S4
Tables S1 to S8
ESI References

Materials and Methods

S1. Material

List of the materials and provenance given in table S1.

S2. Methods

S2.1 Preparation of aqueous two-phase systems

Aqueous two-phase systems were prepared as described in ref.[2-5] Stock solutions of dextran-500 (32 %wt.), PEG-8000 (50 %wt.), PEG-35000 (40 %wt.), and sodium sulfate (1.7 M) were prepared in deionized water. Stock solutions of sodium/potassium phosphate buffer (K/NaPB, 0.5 M), pH 7.4 and sodium phosphate buffer (NaPB, 0.5 M), pH 6.8 were prepared separately. Mixtures of dextran-500 and PEG-35000 or dextran-70 and PEG-8000, and PEG-8000 and Na_2SO_4 were prepared by dispensing appropriate amounts by weight of the aqueous stock solutions of polymers, buffers, Na_2SO_4, salts additives, and nonionic additive (sorbitol, sucrose, and trimethylamine N-oxide) into a 15 mL tube. The final compositions of the aqueous two-phase systems are listed in tables S2 through S5.

The systems of total weight of 12.0 g were vortexed and centrifuged (Beckman GS69 with G.H. 3.8 rotor, Palo Alto, CA, USA) for 60 min at 2,800 RPM (1,300xg) at 23 °C to accelerate phase separation. After centrifugation aliquots from the upper and lower phases were withdrawn for analysis, with the interphase discarded.

S2.2 Solvatochromic studies

The solvatochromic probes 4-nitroanisole, 4-nitrophenol, and Reichardt's carboxylated betaine dye were used to measure the dipolarity/polarizability, π^*, hydrogen bond acceptor (HBA) basicity, β, and hydrogen bond donor (HBD) acidity, α, of the media in the separated phases of ATPS. Aqueous solutions (ca. 10 mM) of each solvatochromic dye were prepared and 10-20 μL of each was added separately to a total volume of 500 μL of a given phase of ATPS. A strong base was added to the samples (~5 μL of 1 M NaOH to 500 μL of a given phase) containing Reichardt's carboxylated betaine dye to ensure a basic pH. A strong acid (~10 μL of 1 M HCl to 500 μL of the phase) was added to the samples containing 4-nitrophenol in order to eliminate charge-transfer bands of the phenolate anion that were observed in some solutions. The respective blank phases without dye were prepared separately. The samples were homogenized in a vortex mixer and the absorption spectrum of each solution measured. To confirm reproducibility, and avoid possible aggregation or other specific interaction effects, the position of the band maximum in each sample was measured in five separate aliquots. A UV-VIS microplate reader spectrophotometer SpectraMax Plus384 (Molecular Devices, Sunnyvale, CA, USA) with a bandwidth of 2.0 nm, data interval of 1 nm, and ~0.5 nm/s high resolution scan acquired the UV–Vis molecular absorbance data. Measured absorption spectra covered the range from 240 to 600 nm. A baseline reference was established by scanning the black phase of ATPS without dye. The wavelength of maximum absorbance in each phase was determined as described by Huddleston *et al.*[6] using PeakFit software package from Systat Software Inc., San Jose, CA, USA, and averaged. Standard deviation for the measured maximum absorption wavelength was ≤0.4 nm for all dyes in all solutions examined.

The maximum observed shifts in three solvents, water, n-hexane, and methanol for different concentrations of 4-nitrophenol with and without HCl, and for Reichardt's carboxylated betaine dye with and without NaOH, corresponded within experimental errors to literature values.

π^*, β and α were calculated from the results of the solvatochromic studies using the methods described by Marcus.[7]

S2.2.1 Determination of the solvent dipolarity/polarizability π^*

The value of π^* was determined from the wave number (ν_1) of the longest wavelength absorption band of the 4-nitroanisole dye using the relationship:

$$\pi^* = 0.427(34.12 - \nu_1) \quad \text{(S1)}$$

S2.2.2 Determination of the solvent hydrogen-bond acceptor basicity β

β values were determined from the wave number (ν_2) of the longest wavelength absorption band of the 4-nitrophenol dye using the relationship:

$$\beta = 0.346(35.045 - \nu_2) - 0.57\pi^* \quad \text{(S2)}$$

S2.2.3 Determination of the solvent hydrogen-bond donor acidity α

α values were determined from the longest wavelength absorption band of Reichardt's betaine dye using the relationship:

$$\alpha = 0.0649E_T(30) - 2.03 - 0.72\pi^* \quad \text{(S3)}$$

The $E_T(30)$ values are based on the solvatochromic pyridinium N-phenolate betaine dye (Reichardt's dye) as the probe, and are obtained directly from the wavelength (λ, nm) of the absorption band of the carboxylated form, as:

$$E_T(30) = (1/0.932)\ [(28591/\lambda) - 3.335] \quad \text{(S4)}$$

S2.3 Analysis of electrostatic properties of the phases

The difference between the electrostatic properties of the coexisting phases is determined in each ATPS by partitioning a homologous series of sodium salts of dinitrophenylated (DNP-) amino acids with the aliphatic alkyl side-chains of the increasing length, alanine, norvaline, norleucine, and α-amino-n-octanoic acid. Partition coefficients of these compounds are presented graphically in Fig. S1, where the logarithms of their partition coefficients are plotted against the length of the side-chain expressed in equivalent number of methylene groups, N_c. The N_c values for the DNP-amino acids used are DNP-ALA Na – 1.31, DNP-norvaline Na – 2.65, DNP-norleucine Na – 3.75, and DNP-α-amino-n-octanoic acid Na – 6.30. Figure S1 shows that the data in each ATPS is as described:[2-4]

$$\log_{10}K^i_{DNP\text{-}AA} = c_i + E_i{*}N_c \quad \text{(S5)}$$

where $K_{DNP\text{-}AA}$ is the partition coefficient of a DNP-amino acids Na-salt; N_c is the equivalent number of CH_2 groups in the side-chain, E and c are constants for a given i^{th} ATPS characterizing the difference between the relative hydrophobicity and electrostatic properties of the phases correspondingly.

S2.4 Interfacial tension measurements

S2.4.1 Formation of pendant drops

Interfacial tension of each ATPS was determined using pendant drop tensiometry.[8] Drops of the lower, denser, phase of a given ATPS were dispensed by a programmable syringe pump from a 100 µL Hamilton glass syringe via a vertically mounted 22-gauge square-ended needle. The needle was lowered until fully submerged in 3-4 mL of the upper, less dense phase of the same ATPS in a custom-made 2.5 cm by 1 cm borosilicate glass cuvette. With frequent stops to avoid snap off,[9] the liquid was dispensed at 1 µL/min, to form a droplet with a volume in the 0.2-0.5 µL range, resulting in a well-deformed (Neumann numbers of the order of 1)[10] stable droplet. Images of the fully formed droplet were taken every 5 seconds over 10 minutes. Figure S2 illustrates examples of pendant drops for various ATPSs. The volume during this time changed by less than 0.5% and

the surface tension, determined as discussed below, from these ~200 images per system was constant within 0.1%. All experiments were conducted at 23 ± 0.1°C.

S2.4.2 Experimental setup

The pendant drop tensiometer setup consists of borosilicate glass cuvette, a 100 µL Hamilton syringe held vertically by a Legato 130 programmable syringe pump from KD Scientific fixed to a stainless steel stand, a Pixelink PL-B776F CCD camera, a Thorlabs, OSL1 High Intensity Fiber Illuminator light source and a glass diffuser. All units were mounted on a linear rail on a Kinetic Systems, Vibraplane 5720E-3036-21 vibration free table. Before each experiment, the enclosure was wiped with methanol to remove any dust. The syringe and cuvette were each cleaned with KOH solution consisting of 24 g of pure water, 24 g of KOH, and 164 g of ethanol, followed by at least three rinses with deionized water and finally with three rinses of HPLC-grade water, and then left to dry completely in a clean environment at room temperature. Images are saved, archived and subsequently analyzed using an Axisymmetric Drop Shape Analysis (ADSA) program.[8]

S2.4.3 ADSA Analysis

The shape of the pendant drop relies on the balance between gravity and interfacial tension. ADSA provides estimates of interfacial tension based on an optimized fit to the silhouette of a fluid droplet as determined by the CANNY algorithm, of the Young-Laplace equation of capillarity:[8]

$$\Delta P = \gamma\left(\frac{1}{R_1} + \frac{1}{R_2}\right) = \Delta P_0 + (\Delta\rho)gz \tag{S6}$$

In this equation, ΔP represents the Laplace, or capillary, pressure across the surface of the drop at any point s; γ represents the droplet interfacial tension; $\Delta\rho$ is the density difference between the two phases; $1/R_1$ and $1/R_2$ are the principle radii of curvature at the point s; g is the gravitational acceleration, and z is the distance along the axis of symmetry between the point s and a reference point where the pressure difference is ΔP_o.

The reproducibility of the interfacial tension values for a given ATPS, which depends on both the experimental set-up and the physical chemistry of each ATPS, was ≤0.002 mN/m for droplets such as those given in Fig. S2. As implied by Eq. S6, the pendant drop tensiometer measures not the surface tension directly but rather the capillary length, λ_c which is defined by:

$$\lambda_c = \left(\frac{\gamma}{g\Delta\rho}\right)^{1/2} \tag{S7}$$

via:

$$\left(\frac{\delta\gamma}{\gamma}\right)^2 = \left(\frac{\delta{\lambda_c}^2}{{\lambda_c}^2}\right)^2 + \left(\frac{\delta(\Delta\rho)}{\Delta\rho}\right)^2 \tag{S8}$$

The standard deviation for the square of the capillary length, over many images of three independent droplets for each ATPS, was:

$$\delta{\lambda_c}^2 = 10^{-9}m^2 \tag{S9}$$

while $\delta(\Delta\rho)$ was typically ten times larger.

Note that in these experiments, the dimensionless Neumann numbers, quantifying the droplet deformation, were of the order of 1, which is expected to give good accuracy in ADSA.[10]

S2.5 Multiple linear regression analysis

The linear relationship between the logarithm of interfacial tension of ATPS with a given ionic composition with or without nonionic additives was confirmed using Eq. 1 presented in the paper.

Data in tables S3 and S4 for ATPS containing 0.01 M K/NaPB, 0.215 M NaCl and 0.215 M $NaClO_4$ additives was fitted by multiple linear regression as described by Ab Rani *et al.*[11] to find each feature-specific coefficient from the p-values. Because only four ATPSs used we have chosen to use the maximum statistical significance value of $p < 0.1$. If three or two coefficients out of four (k_π, k_α, k_β, and k_c) were found to be statistically significant ($p < 0.1$), the correlation was accepted. If one or more values showed a p-value ≥ 0.1, equations with different combinations of coefficients were examined. The equation with a set of coefficients providing p-values <0.1 for all parameters was accepted.

Supplementary Text

S3. Phase diagram

Figure S3 shows the phase diagram of the two coexisting phases for different mixtures of two polymers in water.

The curved line (the binodal curve) separates two regions of polymer mixture compositions. All compositions below the binodal line correspond to a homogeneous single-phase region, while those above the binodal line correspond to the region of two-phase systems. Points representing the compositions of the upper and lower phases lie on the binodal curve. The line connecting the compositions of the two coexisting phases and the overall composition of the system is called a tie line. The length of the tie line decreases as the concentrations of the two polymers in a given ATPS are reduced. At a certain point called the critical point (point C in Fig. S3) the compositions of the two coexisting phases are identical.

In contrast to typical organic solvent-water biphasic systems, any selected pair of polymers in water may form many different pairs of coexisting phases of different compositions and properties. However, any point on the tie line may be achieved by varying the relative volumes of the upper and lowers phases, as shown in Fig. S3 as points A_o, A_1, A_2. It should be emphasized that the interfacial tension value characterizes the system positioned on a given tie-line independent of the ratio of the volumes of the two phases.

Any ATPS with the overall composition close to the binodal line would be extremely sensitive to any changes in such external factors as concentrations of additives (salts or nonionic co-solutes), temperature, etc. This situation is similar to formation of membrane-less organelles of relatively small volumes formed in a relatively large volume of cytoplasm or nucleoplasm.

The so-called tie-line length is commonly used as a measure of the distance of the ATPS composition from the critical point.

The tie-line length, TLL is:

$$TLL = [(\Delta C_P)^2 + (\Delta C_Q)^2]^{0.5} \quad \text{(S10)}$$

where (ΔC_P) is the difference between the concentrations of polymer P in the coexisting phases and (ΔC_Q) is the difference between the concentrations of polymer (or salt) Q in the coexisting phases. The larger the TLL value is, the further away the ATPS composition is from the critical point.

According to multiple authors[12-16] the logarithm of interfacial tension is nearly related to the TLL in various ATPS formed by two nonionic polymers as well as those formed by a single polymer and inorganic salt.

S4 Water perturbation by individual polymers observed with FTIR-spectroscopy analysis

The OH stretch band was analyzed as described in[17] for aqueous solutions of PEG-4000 and Ucon-3930 at same concentrations varied from 0 to 40 %wt. for each polymer. Figure S4 shows an example of the model used for analysis[18] based on the spectra of the OH stretch profile (3000-3700 cm^{-1}) decomposition into five Gaussian sub-bands at 3007 (I), 3225 (II), 3311 (III), 3393 (IV) and 3497 cm^{-1} (V) to fit the spectrum of H_2O.

The Gaussian bands are not exactly representative of specific water groups, which, according to Bakker and Skinner,[19] give rise to asymmetric distributions with longer tails towards lower wavenumbers. Based on their decomposition, sub-band I represents groups with predominantly 4 hydrogen bonds to neighbors. The sub-bands II and III represent mixtures of clusters with 3 and 4 hydrogen bonds, sub-band IV likely represents a mixture of water subpopulations with 3, 2, and 1 hydrogen bonds, and the sub-band V is a population dominated by water clusters with 2 and 1 hydrogen bonds.

The integrated intensities of the sub-bands obtained from the spectral decomposition were used to calculate the relative fractional intensities of the parameters at each concentration of polymer by dividing the intensity of a sub-band by the sum of the intensities of all sub-bands. The data are presented in table S7. The sub-bands III-V gain relative intensities with increasing polymer concentration, while the intensities of sub-bands I and II decrease. The redistribution of these intensities was slightly more pronounced for PEG-4000 relative to Ucon-3930.

Analysis of the relative intensities of the aforementioned sub-bands and the solvent features of water in the same aqueous solutions of the polymers reported previously[20] showed the following relationships:

Every solvent feature, dipolarity/polarizability, π^*, hydrogen bond donor acidity, α, and hydrogen bond acceptor basicity, β, was found to be linearly related to the relative intensity of a particular Gaussian sub-band or a sum of intensities of two or more sub-bands. The coefficients of the linear relationships derived from the IR-data[17] and solvent features of water in solutions of PEG-4000 and Ucon-3930[20] are presented in table S8 together with statistical characteristics for each relationship which may be described by:

$$\text{Solvent feature} = k_0 + k_1 I_1 + k_2 I_2 \qquad \text{(S11)}$$

where I_1 and I_2 are the relative intensities of the sub-bands 1 and 2, and k_0, k_1, and k_2 are constants.

The data in table S7 show that (a) the relative intensity of different sub-bands describe the same solvent features in solutions of PEG-4000 and Ucon-3930, and (b) the relative intensity of different combinations of sub-bands describe different solvent properties in aqueous solutions of the polymers. The overall number of hydrogen bonds formed by different subpopulations of water represented by the particular IR-sub-bands in each relationship are shown in table S8. The data in table S8 imply that changes in the solvent properties of water induced by the polymers are generated by the polymer-specific redistribution of different subpopulations of water in aqueous solutions of the polymers.

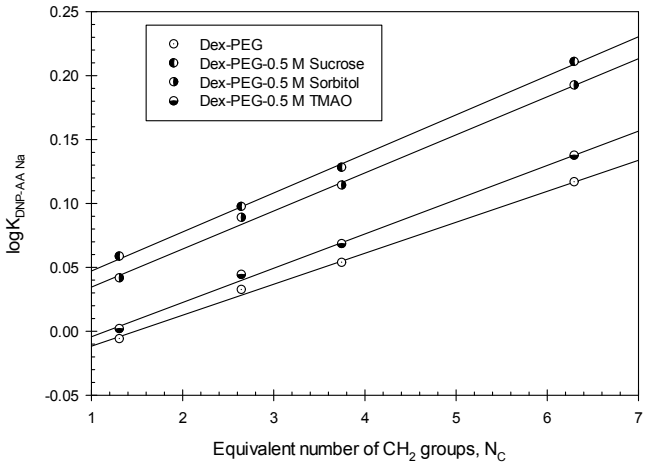

Fig. S1. Logarithm of the partition coefficient value, $K_{DNP\text{-}AA}$, for sodium salts of DNP-amino acids with aliphatic side-chains in 12.0 wt.% dextran-70-6.0 wt.% PEG-8000-0.215 M NaCl-0.01 M K/NaPB, pH 7.4 and 12.0 wt.% dextran-70-6.0 wt.% PEG-8000-0.215 M NaCl-0.5 M osmolyte-0.01 M K/NaPB, pH 7.4 (K/NaPB – sodium/potassium phosphate buffer) aqueous two-phase systems as a function of equivalent length of the side-chain, N_C, expressed in terms of equivalent number of CH_2 units. (Differences between solvent features and electrostatic properties of the coexisting phases and interfacial tension given in table S4).

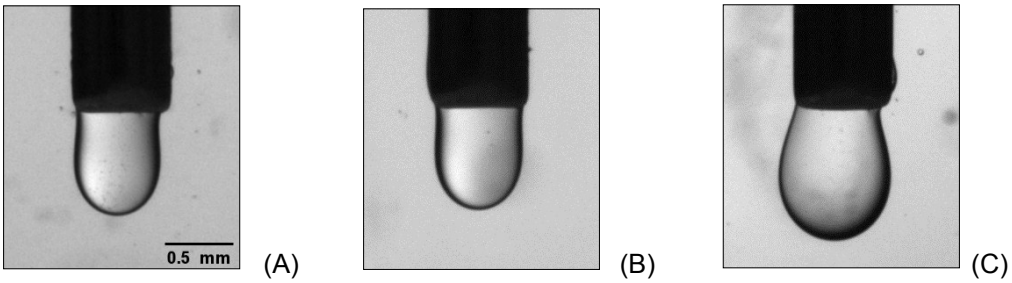

Fig. S2. Pendant drop images for various ATPS (A) dextran-PEG-0.01 M K/NaPB, pH 7.4; (B) dextran-PEG-0.215 M NaCl-0.01 M K/NaPB, pH 7.4; (C) PEG-Na_2SO_4-0.5 M sucrose-0.01 M NaPB, pH 6.8.

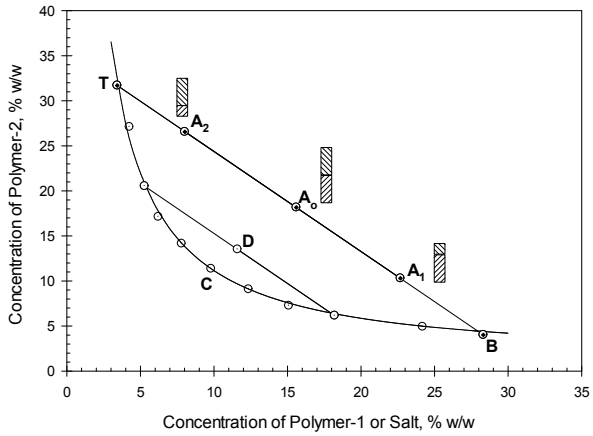

Fig. S3. A typical phase diagram. A_o, A_1, and A_2 represent systems with the three different volume ratios lying on a straight tie-line between compositions of the coexisting phases represented by points B (lower phase) and T (upper phase). Point D represents the total composition of the system lying on the different tie-line. C – critical point determined by extrapolation through the midpoints of several tie-lines.

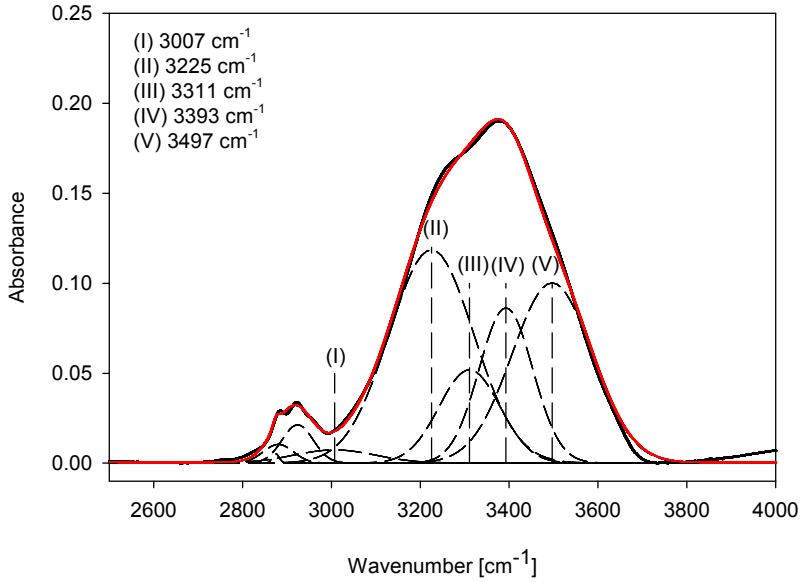

Fig. S4. Spectral decomposition of the OH stretch band profile of water in aqueous solution of 40 %wt. PEG-4000 into sub-bands I-V. Individual sub-bands are accounted for by Gaussian profiles (Data from ref[17]).

Table S1. Materials and provenance.

Material (all from MilliporeSigma, St, Louis, MO	**Average Molecular Weight**	**Lot Number**
Dextran 500 (from leuconostoc mesenteroides)	500,000	86H1463
Dextran 70 (from leuconostoc mesenteroides)	75,000	119945
Polyethylene Glycol	35,000	BCBV8685
Polyethylene Glycol	8000	091M01372V
Sorbitol		SLBF7452V
Sucrose		112343
Trimethylamine N-oxide (TMAO)		BCBT8946
Sodium sulfate		123016
All other salts		ACS grade

Solvatochromic Dyes	**Notes**	**Supplier**
4-nitrophenol	>98% reagent grade	Sigma-Aldrich, Milwaukee, WI
4-nitroanisole	>97%, GC	Acros Organics
Reichardt's carboxylated betaine dye, sodium 2,6-diphenyl-4-[4-(4-carboxylato-phenyl)-2,6-diphenylpyridinium-1-yl]phenolate		Synthesized by method in ref[1]

Table S2. Compositions of dextran-500,000-PEG-35,000-water ATPS and interfacial tension (ITF) values and differences between solvent features of the two phases†.

#	Dextran, %wt.	PEG, %wt.	ITF, σ (μN/m)[b]	Δπ*	Δα	Δβ
1	3.16	2.47	12 ± 1	–0.009 ± 0.002	–0.019 ± 0.002	–0.001 ± 0.002
2	7.78	2.43	37 ± 2	–0.019 ± 0.004	–0.037 ± 0.003	0 ± 0.004
3	9.67	2.42	42 ± 1	–0.020 ± 0.003	–0.045 ± 0.003	0.001 ± 0.003
4	6.21	4.85	82 ± 1	–0.027 ± 0.002	–0.043 ± 0.002	0.001 ± 0.004
5	7.72	4.83	103 ± 6	–0.029 ± 0.002	–0.044 ± 0.002	–0.002 ± 0.002
6	9.60	4.80	150 ± 6	–0.032 ± 0.008	–0.048 ± 0.005	–0.001 ± 0.010
7	9.16	7.16	209 ± 6	–0.036 ± 0.002	–0.051 ± 0.002	0 ± 0.005

†π^*- solvent dipolarity/polarizability; α - solvent hydrogen-bond donor acidity; β - solvent hydrogen-bond acceptor basicity; all differences are calculated as those between values measured in the top phase and those measured in the bottom phase; [b] data from ref[12].

Table S2a. Compositions of dextran-500,000-PEG-35,000-water ATPS and the solvent features of the two phases† in the dextran-500,000-PEG-35,000 ATPS**.**

#	Dextran, %wt.	PEG, %wt.	Top PEG-rich phase			Bottom dextran-rich phase		
			π*	α	β	π*	α	β
1	3.16	2.47	1.105±0.001	1.160±0.001	0.603±0.001	1.114±0.001	1.179±0.001	0.604±0.001
2	7.78	2.3	1.112±0.002	1.114±0.002	0.608±0.002	1.131±0.002	1.151±0.001	0.608±0.002
3	9.67	2.42	1.108±0.001	1.102±0.001	0.610±0.003	1.128±0.001	1.147±0.001	0.609±0.001
4	6.21	4.85	1.113±0.001	1.093±0.001	0.609±0.004	1.140±0.001	1.135±0.001	0.608±0.001
5	7.72	4.83	1.110±0.001	1.085±0.001	0.612±0.001	1.139±0.001	1.128±0.001	0.614±0 .001
6	9.60	4.80	1.104±0.002	1.080±0.002	0.611±0.004	1.136±0.003	1.128±0.003	0.612±0.001
7	9.16	7.16	1.104±0.001	1.059±0.001	0.615±0.003	1.140±0.001	1.109±0.001	0.615±0.002

†π^*- solvent dipolarity/polarizability; α - solvent hydrogen-bond donor acidity; β - solvent hydrogen-bond acceptor basicity.

Table S3. Differences between solvent features† and electrostatic properties‡ of the coexisting phases of 12.0 %wt. dextran-70- 6.0 %wt. PEG-8000-0.01 M K/NaPB ATPSs with and without 0.5 M osmolytes (K/NaPB – potassium/sodium phosphate buffer, pH 7.4; TMAO – trimethylamine N-oxide) and interfacial tension (ITF) values.

Osmolyte	$\Delta\pi^*$	$\Delta\alpha$	$\Delta\beta$	c^b	ITF, μN/m
-	-0.042 ± 0.001	-0.051 ± 0.001	0.006 ± 0.002	0.058 ± 0.003	97.8 ± 0.3
Sucrose	-0.073 ± 0.001	-0.046 ± 0.002	0.023 ± 0.001	0.110 ± 0.001	109.9 ± 0.9
Sorbitol	-0.042 ± 0.001	-0.066 ± 0.001	0.006 ± 0.001	0.090 ± 0.002	121.2 ± 0.7
TMAO	-0.031 ± 0.001	-0.074 ± 0.002	0.009 ± 0.002	0.083 ± 0.002	99.7 ± 3.2

†π^*- solvent dipolarity/polarizability; α - solvent hydrogen-bond donor acidity; β - solvent hydrogen-bond acceptor basicity; all differences are calculated as those between values measured in the top phase and those measured in the bottom phase; ‡c characterizes the difference between the electrostatic properties of the coexisting phases; data from ref[2].

Table S4. Differences between solvent features† and electrostatic properties‡ of the coexisting phases of 12.0 %wt. dextran-70- 6.0 %wt. PEG-8000-0.215 M NaCl-0.01 M K/NaPB and 12.0 %wt. dextran-70- 6.0 %wt. PEG-8000-0.215 M $NaClO_4$-0.01 M K/NaPB ATPSs with and without osmolytes (K/NaPB – potassium/sodium phosphate buffer, pH 7.4) and interfacial tension (ITF) values.

Osmolyte	$\Delta\pi^*$	$\Delta\alpha$	$\Delta\beta$	c^b	ITF, μN/m
0.215 M NaCl					
-	-0.037 ± 0.003	-0.054 ± 0.002	0.002 ± 0.002	-0.036 ± 0.004	105.2 ± 4.7
0.5 M Sucrose	-0.040 ± 0.003	-0.080 ± 0.002	0.004 ± 0.003	0.017 ± 0.002	131.0 ± 1.1
0.5 M Sorbitol	-0.041 ± 0.002	-0.063 ± 0.002	0.007 ± 0.002	0.005 ± 0.0005	128.2 ± 2.0
0.5 M TMAO	-0.033 ± 0.002	-0.065 ± 0.002	-0.019± 0.002	-0.032 ± 0.004	109.7 ± 1.3
0.215 M $NaClO_4$					
-	-0.037 ± 0.002	-0.031 ± 0.003	0.004 ± 0.002	-0.049 ± 0.001	109.4 ± 1.1
0.5 M Sucrose	-0.044 ± 0.002	-0.072 ± 0.003	0.008 ± 0.002	-0.056 ± 0.003	170.3 ± 2.7
0.5 M Sorbitol	-0.040 ± 0.002	-0.067 ± 0.003	0.006 ± 0.002	-0.056 ± 0.009	139.0 ± 2.5
0.5 M TMAO	-0.031 ± 0.003	-0.075 ± 0.003	0.003 ± 0.004	0.0546± 0.0007	116.0 ± 1.0

†π^*- solvent dipolarity/polarizability; α - solvent hydrogen-bond donor acidity; β - solvent hydrogen-bond acceptor basicity; all differences are calculated as those between values measured in the top phase and those measured in the bottom phase; ‡c characterizes the difference between the electrostatic properties of the coexisting phases; data from ref[3].

Table S5. Differences between solvent features† and electrostatic properties‡ of the coexisting phases of 11.1 %wt. PEG-8000-6.33 %wt. Na_2SO_4-0.01 M NaPB ATPSs with and without osmolytes (NaPB – sodium phosphate buffer, pH 6.8) and interfacial tension (ITF) values.

Osmolyte	$\Delta\pi^*$	$\Delta\alpha$	$\Delta\beta$	c^b	ITF, μN/m
-	-0.029 ± 0.003	-0.128 ± 0.004	0.015 ± 0.004	0.445 ± 0.005	43.4 ± 3.8
Sucrose	-0.077 ± 0.005	-0.228 ± 0.007	0.028 ± 0.008	0.670 ± 0.020	234.5 ± 2.7
Sorbitol	-0.046 ± 0.004	-0.248 ± 0.005	0.021 ± 0.008	0.670 ± 0.011	225.8 ± 7.8

†π^*- solvent dipolarity/polarizability; α - solvent hydrogen-bond donor acidity; β - solvent hydrogen-bond acceptor basicity; all differences are calculated as those between values measured in the top phase and those measured in the bottom phase; ‡c characterizes the difference between the electrostatic properties of the coexisting phases; data from ref.[4]

.

Table S6. Solvent properties of water in solutions of individual polymers†.

Medium	Hydrogen Bond Donor Acidity	Dipolarity/polarizability
Pure Water	1.237 ± 0.003	1.096 ± 0.003
Ucon-3930, 30 %wt.	0.766 ± 0.009	1.105 ± 0.003
PEG-4500, 30 %wt.	0.872 ± 0.004	1.119 ± 0.001
dextran-70, 30 %wt.	1.052 ± 0.004	1.157 ± 0.003

† Data from ref.[20]

Table S7. Relative intensities of sub-bands I-V in aqueous solutions of PEG-4000 and Ucon-3930 (data from ref[17]; solvent features of water are from ref[20]). Polymer concentrations are in %wt.

[PEG]	π_i*	α_i	β_i	$I_{3007cm^{-1}}$	$II_{3225cm^{-1}}$	$III_{3311cm^{-1}}$	$IV_{3393cm^{-1}}$	$V_{3497cm^{-1}}$
0	1.096	1.237	0.596	0.0509	0.461	0.0988	0.163	0.226
10	1.109	1.060	0.612	0.0510	0.440	0.0820	0.150	0.270
20	1.112	0.963	0.628	0.0460	0.430	0.0840	0.160	0.270
30	1.119	0.872	0.652	0.0410	0.410	0.0870	0.170	0.290
40	1.124	0.762	0.673	0.0330	0.390	0.0910	0.170	0.310
[Ucon]								
0	1.096	1.237	0.596	0.0509	0.461	0.0988	0.163	0.226
10	1.129	0.996	0.631	0.053	0.446	0.0815	0.155	0.264
20	1.120	0.863	0.656	0.0504	0.441	0.0836	0.157	0.268
30	1.105	0.766	0.684	0.0414	0.419	0.0895	0.166	0.284
40	1.083	0.666	0.708	0.0332	0.397	0.0921	0.174	0.303

Table S8. Coefficients of Eq. S11 and statistical characteristics of each relationship (N – number of experimental points; SD – standard deviation; F – ratio of variance) for aqueous solutions of 0 to 40 %wt. of PEG-4000 and Ucon-3930.

Solvent feature	k_o	k_1	I_1, cm^{-1} †	k_2	I_2, cm^{-1} †	N	r^2	SD	F
PEG-4000									
π*	1.296 ± 0.003	-0.36 ± 0.01	3225	-0.33 ± 0.04	3311	5	0.9989	0.001	883
α	-0.99 ± 0.096	22.2 ± 0.86	3007	11.1 ± 0.97	3311	5	0.9975	0.013	391
β	0.63 ± 0.06	-2.5 ± 0.53	3007	0.40 ± 0.13	3497	5	0.9909	0.004	109
Ucon									
π*	0.60 ± 0.04	4.3 ± 0.31	3007	0.70 ± 0.07	3393 + 3497‡	5	0.9915	0.002	117
α	-10.6 ± 1.4	65.3 ± 6.1	3007	52.03 ± 6.7	3393	5	0.9875	0.035	78.9
β	2.5 ± 0.24	-11.6 ± 1.1	3007	-8.3 ± 1.2	3393	5	0.9898	0.006	97.3

† Relative intensity of the sub-band at the wavelength indicated; ‡ Overall relative intensity of two sub-bands at the indicated wavelengths.

References

1 C. Reichardt, D. Q. Che, G. Heckenkemper, G. Schafer, *Eur J Org Chem*, 2001, **12**, 2343-2361.
2. L. A. Ferreira, P. P. Madeira, V. N. Uversky, B. Y. Zaslavsky, *Rsc Adv*, 2015, **5**, 59812-59822.
3. N. R. da Silva, L. A. Ferreira, J. A. Teixeira, V. N. Uversky, B. Y. Zaslavsky, *J Chromatogr A*, 2019, **1583**, 28-38.
4. N. R. da Silva *et al.*, *J Chromatogr A*, 2015, **1415**, 1-10.
5. L.A. Ferreira, L. Breydo, C. Reichardt, V.N. Uversky, B.Y. Zaslavsky, *J Biomol Struct Dyn*, 2017, **35**, 1055-1068.
6. J. G. Huddleston, H. D. Willauer, R. D. Rogers, *J Chromatogr B*, 2000, **743**, 137-149.
7. Y. Marcus, *Chem Soc Rev*, 1993, **22**, 409-416.
8. S. M. I. Saad, Z. Policova, A. W. Neumann, *Colloid Surface A*, 2011, **384**, 442-452.
9. I. Cohen, M. P. Brenner, J. Eggers, S. R. Nagel, *Phys Rev Lett*, 1999, **83**, 1147-1150.
10. J. Yang, K. Yu, Y. Y. Zuo, Langmuir, 2017, **33**, 8914-8923.
11. M. A. Ab Rani, A. Brant, L. Crowhurst, A. Dolan, M. Lui, N. H. Hassan, J. P. Hallett, P. A. Hunt, H. Niedermeyer, J. M. Perez-Arlandis, M. Schrems, T. Welton, R. Wilding, *Phys Chem Chem Phys*, 2011, **13**, 16831–16840.
12. E. Atefi, J. A. Mann, H. Tavana, *Langmuir*, 2014, **30**, 9691-9699.
13. J. Ryden, P.-A. Albertsson, *J Colloid Interface Sci*, 1971, **37**, 219-222.
14. S. Bamberger, G. V. F. Seaman, K. A. Sharp, D. E. Brooks, *J Colloid Interf Sci*, 1984, **99**,194-200.
15. S. Schurch, D. F. Gerson, D. J. L. Mciver, *Biochimica Et Biophysica Acta,* 1981, **640**, 557-571.
16. D. Forciniti, C. K. Hall, M. R. Kula, *J Biotechnol*, 1990, **16**, 279-296.
17. J. Pavelec, D. DiGuiseppi, B. Y. Zavlaysky, V. N. Uversky, R. Schweitzer-Stenner, *J Mol Liq*, 2019, **275**, 463-473.
18. B. Ratajska-Gadomska, W. Gadomski, *Journal of Chemical Physics*, 2004, **121**, 12583-12588.
19. H. J. Bakker, J. L. Skinner, *Chem Rev*, 2010, **110**, 1498-1517.
20. L. A. Ferreira *et al.*, *J Biomol Struct Dyn*, 2016, **34**, 92-103.